Available online at www.sciencedirect.com
SCIENCE DIRECT®
Journal of Sound and Vibration 290 (2006) 794–819
JOURNAL OF SOUND AND VIBRATION
www.elsevier.com/locate/jsvi

# Active control of payload fairing noise

Steven A. Lane[a,*], Marty Johnson[b], Chris Fuller[b], Arnaud Charpentier[c]

[a]*Air Force Research Laboratory, Space Vehicles Directorate, 3550 Aberdeen Ave, SE, Kirtland AFB, NM 87117, USA*
[b]*Vibrations and Acoustics Laboratory, Virginia Tech, 131 Durham Hall, Blacksburg, VA 24061-0238, USA*
[c]*ESI/Vibro-Acoustic Sciences Inc., 12555 High Bluff Drive, Suite 250, San Diego, CA 92130, USA*

Received 6 July 2004; received in revised form 5 April 2005; accepted 26 April 2005
Available online 19 August 2005

**Abstract**

This work presents adaptive feedforward control using advanced structural–acoustic actuators to reduce the low-frequency acoustic transmission in a sub-scale composite fairing. The actuators, referred to as distributed active vibration absorbers, are multi-resonance devices specifically designed to produce high output forces over a large bandwidth as necessary for payload fairing noise control. Single- and multi-channel control configurations were implemented using external acoustic disturbance levels as high as 130 dB. Design parameters such as sample frequency, control filter length, reference source, and causality/delay were examined to determine impact on performance. The active control system reduced the broadband interior noise levels by up to 5 dB between 70 Hz and 200 Hz, and 10 dB at specific resonances.


## 1. Introduction

Acoustic levels generated by large launch vehicles can exceed 160 dB over a wide frequency range during launch and can pose significant risk to payload launch survivability. Acoustic blankets attenuate the acoustic response above 200 Hz, but are less effective at lower frequencies. In large composite fairings such as those being developed by the Air Force, low-frequency acoustic resonances in the fairing are a concern. The vibro-acoustic launch environment in the

*Corresponding author. Tel.: +505 846 9944; fax: +505 846 7877.
*E-mail address:* steven.lane@kirtland.af.mil (S.A. Lane).

0022-460X/$ - see front matter © 2005 Elsevier Ltd. All rights reserved.
doi:10.1016/j.jsv.2005.04.017

next generation of composite fairings may potentially be more severe because the fairings will be less massive and have less structural damping, both factors that increase noise transmission [1–4].

The primary sources of payload fairing noise are the rocket exhaust plumes. The sound produced tends to be broadband in nature, and propagates up the side of the launch vehicle fairing as plane waves at sharp oblique angles of incidence. Each rocket plume will generate an independent, uncorrelated acoustic source. Active control systems are typically well suited for the 50–200 Hz bandwidth where blankets are less effective. The wavelengths of the plane waves at these frequencies are on the order of 6–1.65 m in length.

The Air Force Research Laboratory has conducted and sponsored many programs over the past few years to investigate innovative approaches to reduce vibro-acoustic loads during launch. Passive approaches using heterogeneous composite blankets, acoustic resonators and reactive/resistive structural dampers are still being developed and investigated [5–8]. In addition to passive approaches, active noise control approaches have been evaluated for mitigating low-frequency vibro-acoustic loads numerically and experimentally. Both feedforward and feedback approaches have been investigated, but the slight performance benefit could not justify the weight penalty. Such approaches used speaker-based controllers to cancel interior noise (feedforward) or to actively damp the low-frequency acoustic resonances of the payload volume (feedback). Significant attenuation was realized (10–12 dB narrowband), but it was not clear if such a control approach would be feasible for the extremely high sound pressure levels encountered during launch. There was also a significant weight penalty for the control system, which consisted of multiple actuators, control hardware, power sources, and cabling [9–11]. Recent demonstrations of active feedback control used a single actuator placed near the fairing nose to actively damp the first two or three longitudinal modes [12–16]. This approach showed considerable promise and continues to be investigated.

Active structural–acoustic control (ASAC) approaches have been successful for reducing turbulent boundary layer noise, propeller noise, and structural vibration in aircraft. In ASAC, structural actuators are used to minimize an acoustic performance metric. Simulations and experimental investigations of ASAC using proof-mass actuators and piezoceramic patch actuators for fairing noise mitigation have shown little potential. It was determined that piezoceramics and proof-mass actuators did not provide adequate control authority for the high sound pressure levels experienced during launch. Typical structural actuators do not provide the necessary stroke, force, or bandwidth at low frequency that is needed for effective application on fairings. Other active control studies considered active damping of structural vibration to reduce acoustic transmission, but little benefit was realized [17,18].

A recently concluded program conducted by the Air Force Research Laboratory in collaboration with Vibro-Acoustic Sciences, Virginia Tech, and Boeing investigated ASAC of a 2.4-m diameter composite cylinder fabricated by Boeing that was a scaled model of a Delta payload fairing. An innovative structural actuator was developed specifically to operate at high sound pressure levels ($\sim$120 dB re 20 μPa). The actuator, known as a distributed active vibration absorber (DAVA), was based on the ''smart foam'' concept developed by Fuller et al. at Virginia Tech for controlling aircraft cabin noise [19–21]. Single- and multi-channel adaptive feedforward control tests were conducted using the Filtered-X LMS control approach, targeting the 70–200 Hz bandwidth. Multi-input, multi-output (MIMO) tests were conducted outside using two walls of sub-woofers to simulate realistic launch loads and conditions. In the following, development of a

structural–acoustic model of the test cylinder is presented, as well as problems that were encountered. The development and testing of the DAVA actuator is then presented. This is followed by a brief overview of the control approach and a discussion of critical design issues. Finally, analytical and experimental results are presented along with important observations and conclusions.

## 2. Theory

### 2.1. Structural–acoustic transmission

The fairing's internal acoustic response can be described as the result of an input disturbance source being filtered by a strongly coupled system comprised of the fairing and the enclosed acoustic volume. Transmission is governed by the coupling of the external acoustic field with the structure, the dynamic response of the structure, the coupling of the structural response to the acoustic volume, and the dynamics of the acoustic volume. Gardonio et al. provide an excellent analytical derivation of structural–acoustic transmission based on a cylinder that is very much applicable to the fairing noise problem [22].

At structural resonances, energy is transmitted efficiently due to the large out-of-plane motion. Damping of structural modes can significantly reduce transmission at these frequencies. The internal acoustic volume also exhibits resonant behavior, and if a structural mode is proximal to an acoustic mode, noise transmission will be relatively high. Damping acoustic resonances is very effective in reducing the overall internal response, but as stated earlier, it is difficult to add damping to low-frequency acoustic modes. Adding mass to the fairing is not a desirable noise control technique. Although effective, one typically wants to reduce the mass of non-payload items in order to reduce the overall cost of the launch.

As presented in the work by Gardonio et al., noise transmission can also be reduced by targeting and attenuating the response of specific structural modes that efficiently radiate into the fairing interior. The modal response of the structure is essentially ''reconfigured'' such that structural–acoustic coupling is reduced by localized impedance loading of the fairing using passive or active means. The control approach presented in this paper uses all three of these mechanisms to reduce noise transmission: structural damping, acoustic damping, and modal reconfiguration.

### 2.2. The fairing model

Throughout this project, considerable effort was devoted to modeling and understanding the structural–acoustic dynamics governing noise transmission through the composite cylinder testbed, which is shown in Fig. 1. The test article was essentially a simply supported right cylinder of radius 1.226 m (48.25 inches) with height of 2.793 m (110 inches), fabricated using two external graphite epoxy layers, a honeycomb core, and two interior graphite epoxy layers. The cylinder mass was approximately 80 kg (176 lbs). Both ends were capped using thick, structurally reinforced plywood end plates (226 kg) that were fastened to the cylinder and designed to minimize transmission of acoustic energy, since it was desired that the dominant structural–acoustic transmission path be the composite cylinder only. Although real fairings do

Fig. 1. Composite cylinder used for ASAC experiments.

have features such as access panels, ports, and separation rails, that level of realism was not necessary for the present study.

Models of the composite structure and acoustic volume were made and validated. The goal was to develop coupled models accurate to 200 Hz for controller design and simulation purposes. COSMIC NASTRAN was used to perform normal modes analysis and obtain mode shapes and natural frequencies of the cylinder structure. All frequencies below 1000 Hz were computed, but only the first 131 modes were used (up to 300 Hz) for computing transfer functions. The recovery points and loads were specified in Matlab, where transfer functions were computed [23]. Measurements of drive point accelerance and shaker-to-accelerometer transfer functions were

used to validate the structural model. The spatially averaged response from a small electromagnetic shaker to 150 accelerometers (located as shown in Fig. 2) is given in Fig. 3 and compared to the response computed from the validated numerical model. Measurement uncertainty and experimental uncertainty was estimated to be less than $\pm 0.5$ dB based on sensor specifications and test repeatability. The drive point accelerance is shown in Fig. 4. The numerical model corresponded reasonably well to the experimental measurements given the relative complexity and non-uniformity of the structure and the uncertainty in structural parameters.

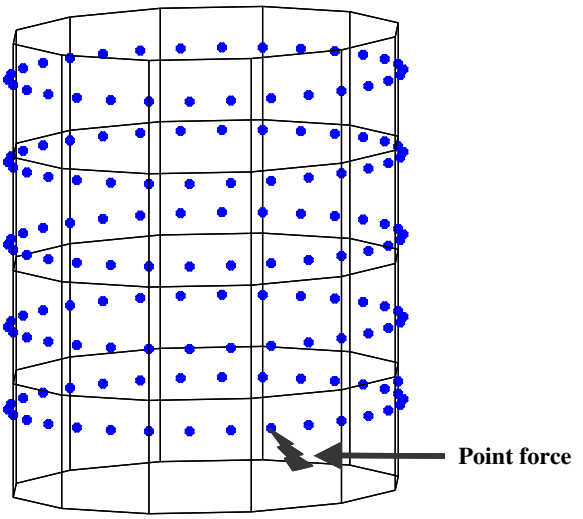


Fig. 2. Shaker and accelerometer locations used for validation of the structural model.

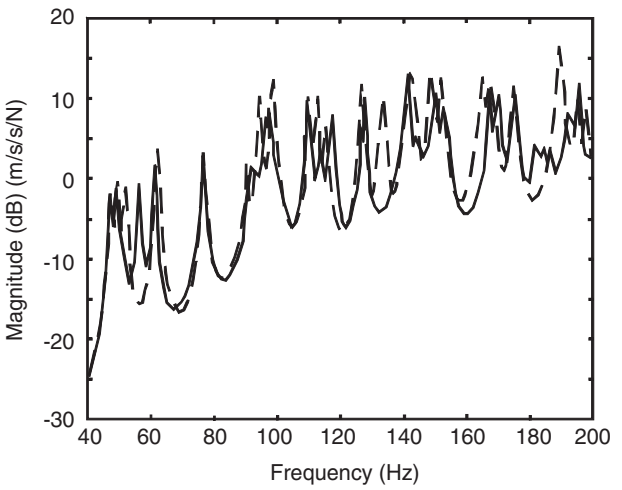


Fig. 3. Comparison of spatially averaged structural response from a point force loading: —, experimentally measured; – –, model prediction.

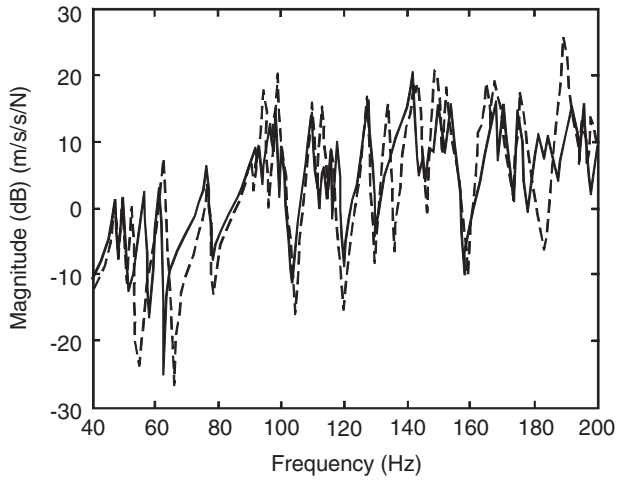


Fig. 4. Drive point structural response: —, experimentally measured; ––, model prediction.

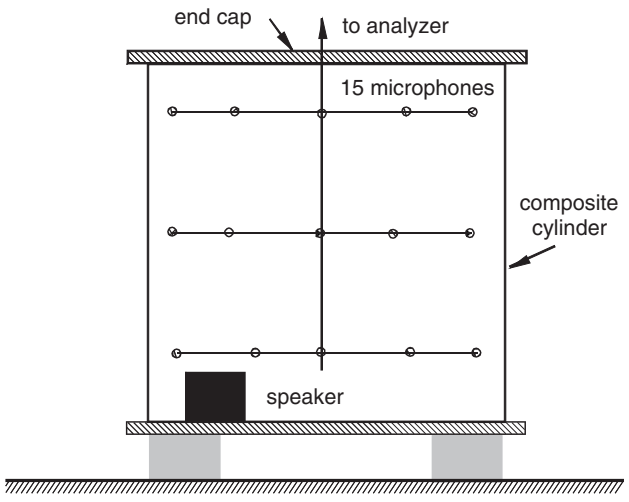


Fig. 5. Schematic of sensor/actuator locations used for validation of the acoustic model.

However, tuning of the model did not yield the level of correlation necessary for developing an accurate coupled model.

The interior volume was modeled using COMET Finite Element. All modes with frequencies below 650 Hz were computed, but only the first 59 modes were used (up to 300 Hz) for computing transfer functions. The mesh spacing was set so that there were at least 6 nodes per wavelength at the highest frequency of interest. Transfer functions measured from a sub-woofer in the cylinder to 15 microphones placed throughout the cylinder interior were used to validate the acoustic model. Fig. 5 shows the experimental setup. The sub-woofer was instrumented with an accelerometer attached to the diaphragm, which served as a reference signal for transfer function

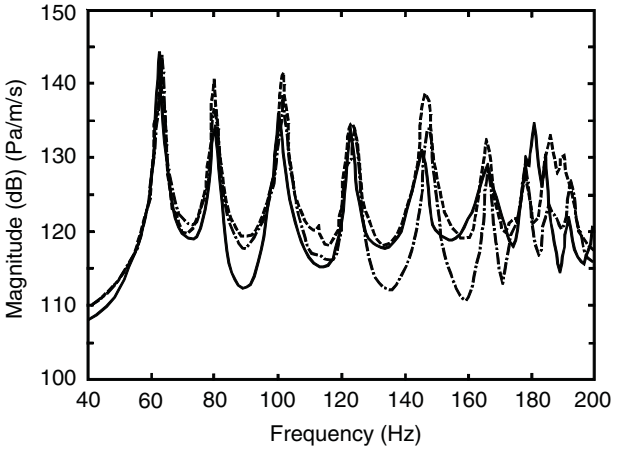


Fig. 6. Comparison of the validated acoustic model to the measured transfer functions: —, averaged measured microphone response; – · –, averaged model microphone response; – –, spatially averaged acoustic response from model.

measurements. The accelerometer output was integrated to velocity. It was assumed that the loudspeaker had negligible impact on the acoustic volume and that the cone was radiating as a piston (low-frequency approximation). A data analyzer system was used to drive the speaker with band-limited random noise, measure the sensor signals, and compute frequency response functions (FRFs). The measurement uncertainty was estimated to be less than $\pm 0.1$ dB. Fig. 6 presents a comparison of spatially averaged, measured transfer functions to those computed from the updated model. Also given in Fig. 6 is the model response averaged over the entire acoustic space using the pressure response at each node. Transfer functions show good agreement between model and experiment up to about 140 Hz. From Fig. 6, it is observed that the fundamental acoustic resonance (longitudinal mode) occurred at approximately 62 Hz. All acoustic modes in the bandwidth were lightly damped.

The structural and acoustic sub-systems were coupled using a modal interaction approach in Matlab [24]. Validation of the coupled structural–acoustic model was difficult due to the uncertainty of the boundary conditions, specifically that due to the end-caps. Although the end-caps were made very bulky, they still remained a transmission path and it was necessary to ultimately include them in the model as flexible members. Several attempts to develop an accurate coupled model were made by using a variety of methods to improve model and experiment agreement. However, the agreement between models and experiment was poor.

Damping material was added to the cylinder to more closely match the actual acoustic damping of a launch vehicle with a payload and reasonable blanket treatment. This was accomplished by making the reverberation time in the cylinder match the reverberation time in a similar sized fairing. Approximately 50% of the total interior surface of the cylinder was lined with 5-cm (2-inch) thick melamine foam as shown in Fig. 7. Even with the addition of the foam material, the acoustic modes that dominated the low-frequency response remained lightly damped with damping values of less than 5% of critical.

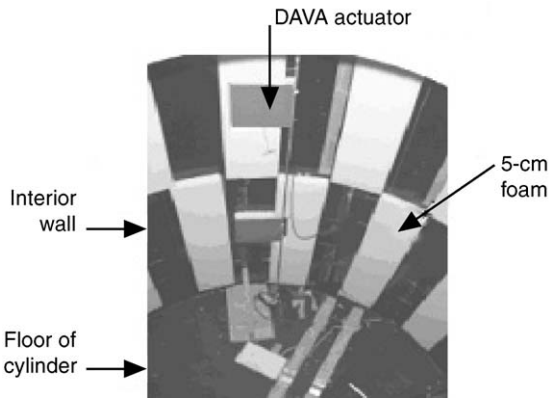


Fig. 7. Acoustic foam applied to the cylinder interior.

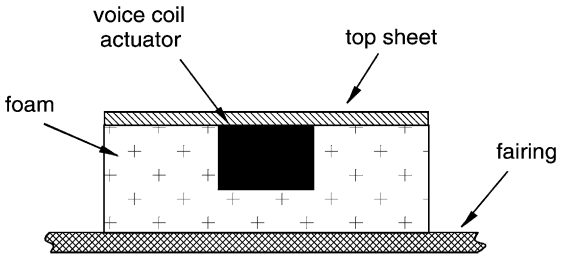


Fig. 8. Schematic of high output DAVA concept.

### 2.3. Actuator development (DAVA)

A key challenge of this program was to develop a structural actuator with enough control authority for realistic disturbance levels. The actuator needed to function across the bandwidth of about 50–200 Hz, and yet remain lightweight, small, and operate on low voltages with minimal power requirements in order to be feasible for fairing applications. The actuator developed under this program used a stiff, lightweight panel, such as a honeycomb or Nomex sheet, which was attached to a compliant foam layer and driven by a voice-coil actuator embedded within the foam layer. This yielded a "distributed" structural actuator that was then attached to the cylinder wall by adhesive. This actuator provided: (1) structural damping by coupling to the structure, (2) a force input to the structure, functioning like a tuned vibration absorber to control radiating modes of the structure, and (3) acoustic damping. Nearly all of the mass of the actuator came from the voice-coil actuator. Several iterations of the actuator were made in order to achieve the necessary force and stroke output to drive the cylinder at high levels. A schematic of a DAVA is given in Fig. 8. Fig. 9 compares the blocked force output from an early DAVA design used for aircraft to the final design used on the composite cylinder (fairing). The final design used a lighter, denser magnetic core with voice-coil windings optimized to reduce heating.

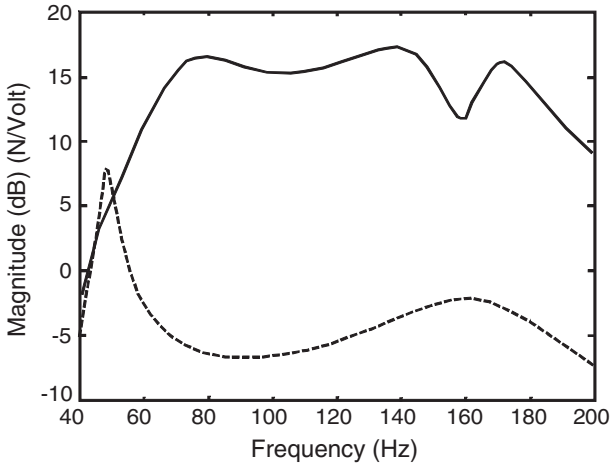


Fig. 9. Comparison of DAVA prototype blocked force responses: —, response of a fairing actuator; – –, response of an aircraft actuator.

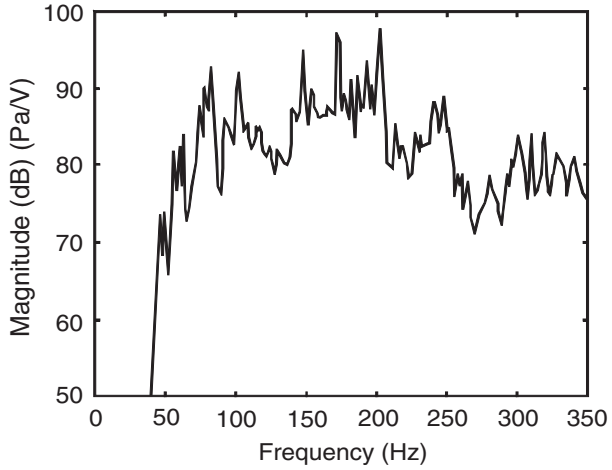


Fig. 10. Acoustic output measured from a single DAVA mounted in the composite cylinder test structure.

A single prototype DAVA was tested in the cylinder by measuring the acoustic response in the cylinder as a function of applied voltage. The internal cylinder response was measured and averaged over 36 microphones and is presented in Fig 10. The results show that the effective bandwidth of the actuator was about 80–200 Hz, with peak outputs of up to 96 dB re: 20 μPa at 1 V (0–350 Hz). The improved force output and bandwidth of the DAVA was a critical achievement enabling control at realistic disturbance levels.

The linearity of the DAVA was also investigated. The force output as a function of applied voltage was inferred from an accelerometer attached to the top plate (measurement uncertainty was less than $\pm 0.1$ dB). The force output was only computed for the design bandwidth, which was

50–200 Hz in this case. The force output is plotted as a function of increasing power in Fig. 11. The DAVA remained linear up to about 20 W, and eventually overheated and failed at approximately 37 W. In each test case, the DAVA was driven with band-limited random noise for 30 s and then allowed to cool for 5 min.

### 2.4. Control approach

The control approach used in this work is referred to as ASAC because structural actuators were being used to minimize an acoustic performance metric, i.e. the error signal was the response from microphones in the cylinder. Feedforward controllers have been used to reduce cabin noise in aircraft, which is a problem similar to the fairing problem except the disturbance loads are different. Adaptive feedforward controllers have the advantage that they are adaptive—they do not rely on static control laws and can adapt to changes in the system. Since adaptive feedforward controllers have never been applied to the fairing problem, there are several important issues that must be considered to evaluate feasibility, including reference sensors, causality, control authority, convergence, stability, power requirements, and performance (noise reduction).

The controllers implemented in these tests used the Filtered-X Least Mean Squares (FXLMS) algorithm [25–27]. FXLMS controllers use finite-impulse response (FIR) filters for control and have the architecture shown in Fig. 12. FXLMS is a gradient-based convergence algorithm, where

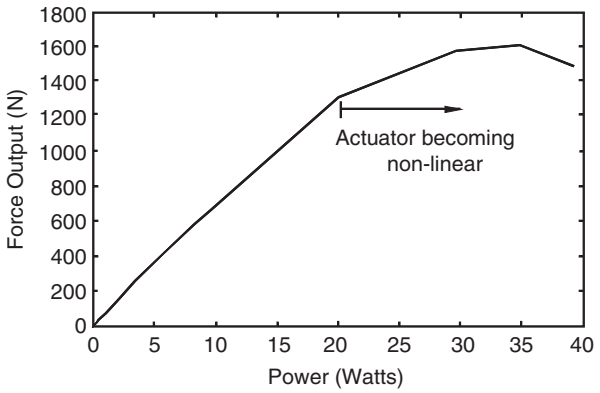


Fig. 11. Linearity of a single DAVA as a function of power.

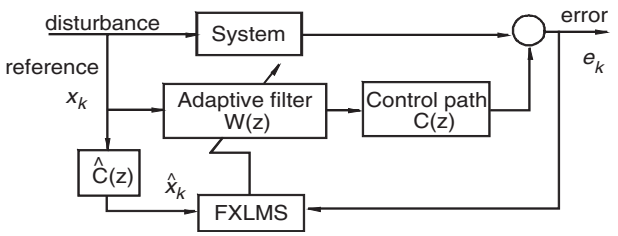


Fig. 12. Block diagram of the Filtered-x LMS control algorithm.

the performance index can be defined as the measured acoustic response in the fairing. For broadband control, the control filter size, denoted as $N$, is increased to adequately capture the dynamics in the bandwidth. For a single-channel controller, the control filter is essentially a vector of scalar coefficients, $\mathbf{w}_k$, that is multiplied with a vector of previous sampled values of a reference signal, $\mathbf{x}_k$, to produce the control signal:

$$\text{control signal} = \mathbf{w}_k \cdot \mathbf{x}_k, \tag{1}$$

where $k$ indicates the discrete time step. The control filter can be initialized to zero and allowed to update to convergence. However, pre-converged control filters can also be used in a re-start configuration. The control filter weights are updated by

$$\mathbf{w}_{k+1} = \mathbf{w}_k - \mu \hat{\mathbf{x}}_k e_k. \tag{2}$$

In Eq. (2), $\mu$ is the convergence factor, $\hat{\mathbf{x}}_k$ is the filtered-$x$ signal, and $e_k$ is the sampled error signal. The transfer function between the control actuator and the error sensor is represented in Fig. 12 as $\mathbf{C}(\mathbf{z})$. An FIR model of $\mathbf{C}(\mathbf{z})$, denoted as $\hat{\mathbf{C}}(\mathbf{z})$, is computed prior to control by driving the actuators with band-limited random noise and measuring the sensor output. The Least Mean Squares (LMS) algorithm is used to converge $\hat{\mathbf{C}}(\mathbf{z})$ to a model of $\mathbf{C}(\mathbf{z})$. This process is called system identification [28,29]. The dynamics in the bandwidth determine the size of the filter needed to adequately represent $\mathbf{C}(\mathbf{z})$. The filtered-$x$ signal is formed by convolving the sampled reference signal, $\mathbf{x}_k$, with $\hat{\mathbf{C}}(\mathbf{z})$. The rate of convergence is determined by the "convergence factor", $\mu$, which is limited by controller stability. There are analytical approaches that can be used to compute the maximum value of the convergence factor based upon the eigenvalue spread of the control path dynamics, but these are rarely accurate. In practice, a suitable value of the convergence factor is determined by trial and error by starting with a small value and increasing until (marginal) instability occurs in order to determine the stability bounds. The system is then implemented at approximately 80% of this value to allow some stability margin. This controller approach can be extended to multiple control channels as presented in the references.

### 2.5. Reference signals

The reference signal used to compute the control signal must be coherent with the disturbance acting on the system; in our case, the acoustic disturbance load impinging on the cylinder. The ability of the controller to attenuate the disturbance depends on the coherence between the reference and the disturbance. Also, there must be adequate time between samples for the computations, since the FIR filters must be multiplied with sampled-data vectors. The number of computations determines the maximum sampling rate of the controller. The time required for the controller to sample the reference, compute the control signal, and send the control signal through the actuator to the system must be less than the time it takes for the same corresponding disturbance sample to propagate through the system. The ability of the controller to stay ahead of the disturbance in this regard is referred to as controller causality. If the control delay is greater than the propagation time of the disturbance through the system, then the controller will never be able to "catch up", and performance will be limited. It is reasonable in some cases to use an accelerometer attached to a structure as a reference signal in ASAC. However, by placing a microphone in the impinging sound field, a slight advantage (referred to as phase-lead) is gained

in that the reference is more "upstream". In some tests that follow, the pre-amp signals driving the disturbance sources were used as references, which maximized controller phase-lead. For a real application, an accelerometer or other structural vibration sensor, or a flush mounted microphone would be reasonable reference sensors, as both provide signals coherent to the disturbance. As noted, by moving the sensor closer to the disturbance source, a better understanding of the "best case" performance should be obtained.

Both single-input, single-output (SISO) and MIMO configurations were tested under different loading conditions. In an MIMO implementation, the computational load increases at a rate nearly proportional to the square of the number of channels. Having more control channels facilitates "global" control, meaning that reduction is achieved throughout the entire system. Single-channel controllers typically only provide a "local" zone of reduction proximal to the error sensor. At some point, the computational ability of the digital signal processor (DSP) is exceeded and a trade-off between the number of channels, FIR filter lengths, sample rate, and ultimately performance must be made.

## 3. Experimental setup

SISO tests were conducted inside an acoustic test facility and outside in an open field. The tests conducted inside were more repeatable than outside tests, since test conditions could be better controlled. The disturbance loads for the indoor tests consisted of direct and reverberant acoustic fields (the lab had scattering and damping surfaces to reduce the influence of room modes). Outdoor tests were more representative of launch conditions, since the acoustic disturbance was directional and included ground reflections.

All SISO tests were performed at relatively low disturbance levels, which produced approximately 80 dB inside the composite cylinder (re: 20 μPa, variation from test-to-test was less than $\pm 2$ dB, 0–200 Hz). The SISO test arrangement is illustrated in Fig. 13. A single microphone was placed approximately 23 cm from the cylinder and used as a reference sensor [30]. In some tests, the microphone was moved further "upstream," i.e., closer to the speaker (61 cm

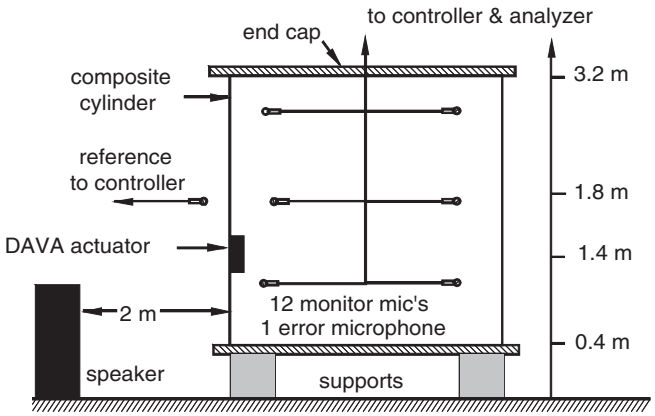


Fig. 13. Experimental setup for the SISO experiments.

from the cylinder). A single 45.6 cm (diaphragm diameter) sub-woofer mounted in a closed cabinet was used as the disturbance source [31]. A single DAVA (24 cm × 24 cm) was attached to the inside wall of the cylinder as indicated in Fig 13. A small, commercial-off-the-shelf power amplifier (maximum power output of approximately 30 W) was used to drive the DAVA. A single error microphone [30] was placed inside the cylinder. During the SISO tests, the microphone was moved around to different locations to observe the effect on performance. Twelve "monitor" microphones [30] were placed in the cylinder to measure the global performance of the controller. A digital signal analyzer was used to generate band-limited random noise that was input to the disturbance sub-woofer. The same signal analyzer was used to measure time- and frequency-domain data from which closed-loop performance was computed. A Texas Instruments TMS320C40 (Quad) DSP housed in a Pentium-based PC was used to compute the system identification and to implement the controller. Cabling for sensors and the actuator was put through a small tube through the center of the top end-cap. This tube was plugged with foam rubber as much as practical to prevent flanking.

All MIMO tests were conducted outside in an open field near the Virginia Tech airport in Blacksburg, Virginia. The external disturbance was generated using two speaker banks, each bank consisting of 8 sub-woofers (NEOX B-1) located on either side of the cylinder as shown in Fig. 14. During tests, the speaker banks were about 1.5 m from the composite cylinder. The sub-woofers were driven by one random noise input generated by the signal analyzer. Some tests used two uncorrelated random signals, both of which were generated by the signal analyzer. Eight Crown MA 5002 power amplifiers (two channels each) were used to drive the sub-woofers, each providing 2500 W per channel.

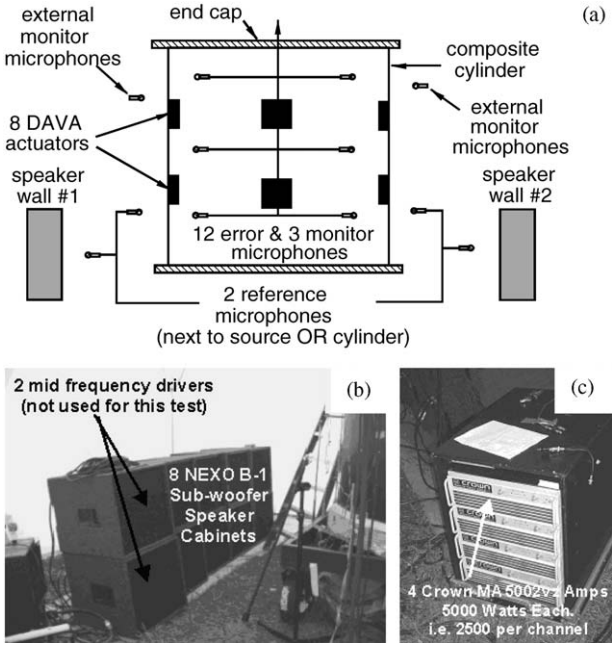


Fig. 14. Experimental setup for the MIMO experiments: (a) schematic diagram; (b) wall of speakers used as disturbance source; (c) rack of power amplifiers.

Four external microphones [30] were used to monitor the disturbance levels. In some tests, one of the external microphones was used as a reference sensor, and in some tests, two of the microphones were used as reference sensors. No more than two reference sensors were deemed necessary because at most two uncorrelated disturbance signals were used. Originally, all of the external microphones were placed about 10 cm from the cylinder wall, which offered a reasonable measurement of the impinging disturbance. However, in some control tests, the reference microphones were moved closer to the disturbance sources to investigate the impact of different lead-times in the control path and the corresponding effect on closed-loop performance.

Fifteen microphones [30] were mounted to a microphone tree inside the cylinder. The controller used 12 of the microphones as error sensors (summed to form a single error metric for updating the controller) and three were used exclusively as monitoring sensors for measuring global performance.

The approximate positioning of the DAVA actuators (24 cm × 24 cm) is shown in Fig. 14. Two rings of four actuators were mounted inside the cylinder. The upper ring was approximately 90 cm from the top and the lower ring about 90 cm from the bottom with angular separation of 90°. Actuator and sensor cabling was put through the same port in the top end-cap that was used for the SISO tests. The MIMO controller was implemented on the same Quad C40 DSP as used for SISO tests.

## 4. Results

### 4.1. SISO tests

An initial measurement was made to compare the external disturbance and the resulting internal acoustic response. A single disturbance sub-woofer was driven with band-limited random noise by the spectrum analyzer (0–300 Hz), and the responses at an external microphone and an internal microphone were measured. The power spectrums of the measured signals are shown in Fig. 15. The measured signals demonstrate how the coupled structural–acoustic system ''filtered'' the disturbance. The internal microphone response exhibited narrow bands of large amplitude, indicative of acoustic resonances. The internal spectral content below 50 Hz was less than the external spectral content by approximately 20 dB. At frequencies above 200 Hz, the internal response was nearly equivalent to the external disturbance.

System identification was performed using the LMS algorithm to identify the control path indicated in Fig. 12 as **C(z)** prior to controller implementation. In all of the SISO tests, the control filters were initialized to zero. Details of the environment, reference signal, sample rate and filter size for several representative tests are given in Table 1. The sample rate for the DSP was between 600–900 Hz. This permitted system identification and control filters between 255 and 500 coefficients.

Table 1 also gives the closed-loop reduction computed over the bandwidth of 0–200 Hz. The closed-loop responses measured at the 12 monitor microphones were spatially averaged to determine global performance. Local reduction was determined from the error microphone. The results varied from as much as 5.88 dB of local reduction (case 11) to a net global increase of 1.45 dB (case 4a). In each test, the controller was able to achieve local control (1.36–5.88 dB), but

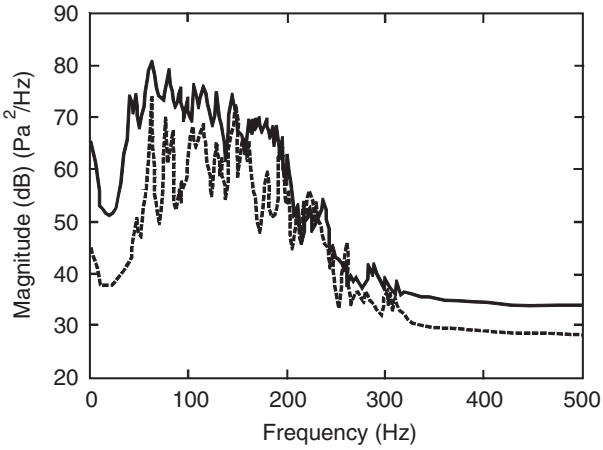


Fig. 15. Power spectrums of microphone measurements for a band-limited random noise disturbance: —, external (reference) microphone; – –, internal (error) microphone.

Table 1
Summary of SISO low-level test cases

| Test ID | Test environment | Reference sensor | Sample rate (Hz) | # FIR coefs | Reduction (dB) | |
|---|---|---|---|---|---|---|
| | | | | | Local | Global |
| 1 | Inside | External mic (23 cm from cylinder) | 900 | 255 | 1.36 | 0.25 |
| 2 | Inside | External mic (23 cm from cylinder) | 750 | 255 | 4.49 | −1.37 |
| 3 | Inside | External mic (23 cm from cylinder) | 600 | 255 | 3.29 | −0.04 |
| 4 | Inside | External mic (23 cm from cylinder) | 800 | 500 | 3.93 (a) | −1.45 (a) |
| | | | | | 4.77 (b) | −1.26 (b) |
| 5 | Inside | External mic (23 cm from cylinder) | 800 | 500 | 2.35 (a) | −0.22 (a) |
| | | | | | 2.76 (b) | −0.41 (b) |
| 6 | Inside | External mic (23 cm from cylinder) | 800 | 500 | 2.86 (a) | 0.20 (a) |
| | | | | | 2.76 (b) | 0.14 (b) |
| 7 | Inside | External mic (23 cm from cylinder) | 600 | 500 | 2.15 | −0.36 |
| 8 | Outside | External mic (23 cm from cylinder) | 700 | 500 | 3.10 | −0.84 |
| 9 | Outside | External mic (61 cm from cylinder) | 700 | 500 | 2.88 | −0.32 |
| 10 | Outside | External mic (61 cm from cylinder) | 700 | 500 | 2.57 | −0.15 |
| 11 | Outside | Disturbance speaker voltage | 700 | 500 | 5.88 | −0.54 |

almost always increased the global response. Tests 4–6 show results for six independent control tests using the same controller parameters, but taken at different times. This illustrates the variability of the converged solutions and the test-to-test variation. Tests conducted outside produced similar levels of performance as tests conducted inside. There was no clear benefit to using a higher sample frequency (900 Hz) instead of a lower sample frequency (600 Hz). There was no clear advantage using 500 FIR filter coefficients instead of 255 coefficients. Moving the

reference microphone closer to the disturbance speaker produced no appreciable improvement. Using the disturbance signal from the analyzer that was used to drive the sub-woofer, i.e., the "ideal" reference scenario, did provide the highest observed local reduction, but yielded no global reduction.

Figs. 16 and 17 show the measured open- and closed-loop power spectral density plots (dB re: 20 μPa) for test 8, for the error microphone and the monitor microphones, respectively. Fig. 16 shows that the SISO controller was effective over the bandwidth of 140–160 Hz, where the largest open-loop magnitude occurred. Reduction was also observed from 75–90 Hz. Spillover was observed below 60 Hz. The overall local response decreased by about 3.1 dB, which is approximately 42% (rms). Fig. 17 shows that reduction at the error microphone does not

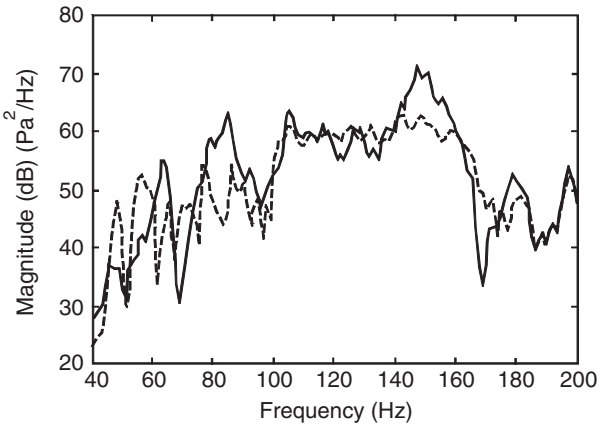


Fig. 16. Power spectral density of the error microphone for a representative SISO test case: —, open-loop measurement; –– closed-loop measurement.

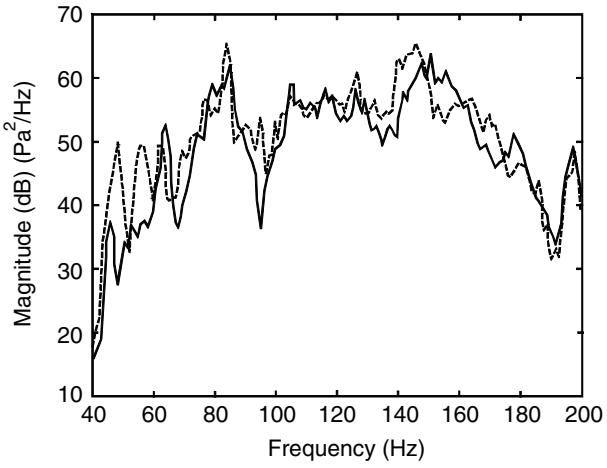


Fig. 17. Power spectral density of the spatially averaged monitor microphones for a representative SISO test case: —, open-loop measurement; –– closed-loop measurement.

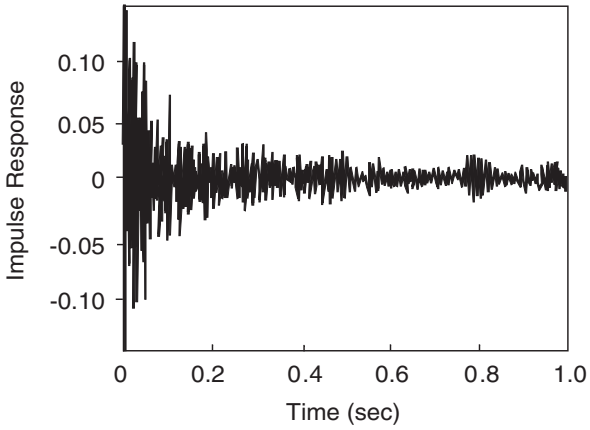


Fig. 18. Computed optimal Wiener filter for the measured SISO system.

indicate global reduction. In fact, the global response over 140–160 Hz and around 80 Hz increased. Spillover was also measured at low frequency. The overall global (0–200 Hz) response increased by 0.84 dB, an increase of approximately 10% (rms).

For this test case, a small resistor (less than 1 Ω) was placed in series with the DAVA, and the current and voltage through the DAVA were measured. After the controller had converged, the voltage applied to the DAVA was determined to be 0.98 V (rms) and the current 0.24 A (rms), or 0.235 W (at 80 dB internal acoustic response).

About 1–3 min were required for the SISO controllers to convergence. The convergence time was roughly 100–200 times the FIR filter length (#FIR coefficients * sample period). While this may be acceptable for a steady-state problem, it is not acceptable for the fairing problem. To investigate the impact of reducing the filter length in order to reduce convergence times, an optimal FIR controller was computed off-line using system identification models taken from experiments. The ''best case'' reduction was computed using optimal (Wiener) filters of varying lengths [32]. For a 1 s filter, the maximum achievable local performance was 15 dB (global performance was not computed). The impulse response of the optimum filter is given in Fig. 18. The impulse response required longer than 1 s to completely decay to zero. Fig. 19 shows the predicted effect of reducing the length of the optimal filter. Reducing the filter duration by 50% resulted in a 4 dB loss of performance. Reducing further to $\frac{1}{4}$ second resulted in a loss of 7 dB. This illustrates the trade-off between closed-loop performance and convergence speed.

### 4.2. MIMO tests

Most MIMO control tests were performed using an external disturbance level of approximately 105 dB (computed over 31–325 Hz). The final MIMO tests (tests 6–8) were performed at increasing disturbance levels, finally achieving about 130 dB. Fig. 20 shows the power spectrums (computed over third-octave bands) of the spatially averaged external microphone measurements. The disturbance rolled off below 63 Hz and above 200 Hz. The controller setup and parameters for each test case is given in Table 2. The closed-loop performance was computed for the bandwidth of 70–200 Hz.

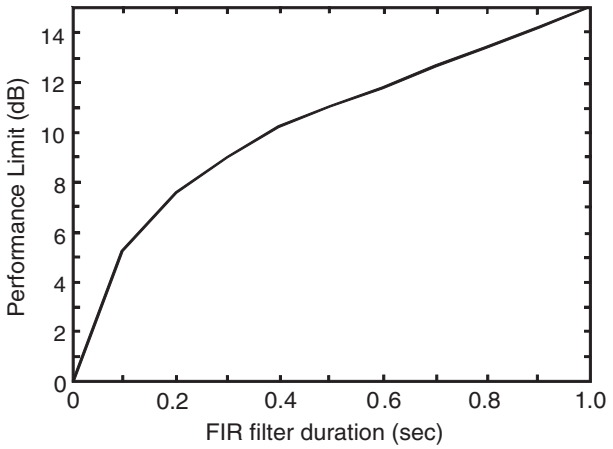


Fig. 19. Plot of performance limit as a function of FIR control filter duration.

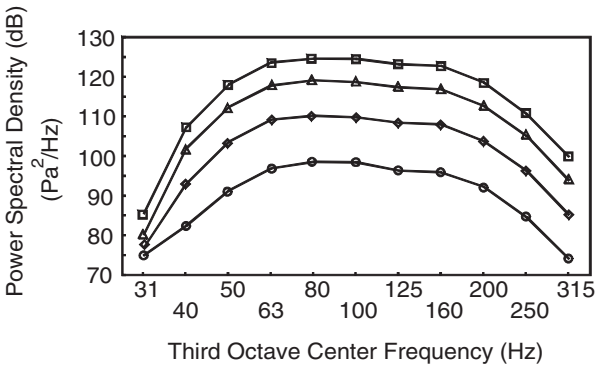


Fig. 20. Exterior sound pressure levels in one-third octave frequency bands from MIMO tests: -○-, 105 dB; -◇-, 117 dB; -△-, 125 dB; -□-, 130 dB.

Table 2
Overall MIMO feedforward tests results

| Test ID | | 1 | 2 | 3 | 4 | 5 | 6 | 7 | 8 |
|---|---|---|---|---|---|---|---|---|---|
| Number of disturbances | | 1 | 1 | 1 | 2 | 2 | 2 | 2 | 2 |
| Exterior level (dB) (31–325 Hz) | | 105 | 104 | 104 | 100 | 101 | 117 | 125 | 130 |
| Number of references | | 1 | 1 | 1 | 2 | 2 | 2 | 2 | 2 |
| Reference type | | ideal | mic near cylinder | mic near disturbance | ideal | mic near disturbance | ideal | ideal | ideal |
| Broadband attenuation | Error mics | 9 | 1.9 | 3.7 | 9.3 | 4.9 | 7.9 | 6.6 | 5.7 |
| (dB) 70–200 Hz | Monitor mics | 3.4 | 0.4 | 1.5 | 7.7 | 4.7 | 7.2 | 6.8 | 6.1 |
| DAVA Power consumption (Watts) 40–300 Hz | | 0.08 | 0.007 | 0.01 | 0.04 | 0.03 | 1.7 | 16 | 25 |
| Convergence time (min) | | $>5$ | $>5$ | $>5$ | $>5$ | $>5$ | $>5$ | $>5$ | $<1$ |

The MIMO controllers used a sample frequency of 700 Hz. The 8 input × 12 output transfer matrix used to represent $\hat{\mathbf{C}}(\mathbf{z})$ used FIR filters of 255 coefficients each. The control filter matrix (8 actuators × 1 reference and 8 actuators × 2 references in some cases) also used 255 coefficients for each FIR. Tests 1–3 were conducted using only one random input signal for all sub-woofer channels. These tests also used a single reference signal for the FXLMS algorithm. For test 1, an ideal reference was used, which was simply the disturbance input applied to the sub-woofers. This provided 9 dB of attenuation at the error microphones (local control, spatially averaged), and 3.4 dB of reduction at the monitor microphones (global control, spatially averaged). For test 2, a microphone near the fairing was used as a reference. The corresponding local reduction was about 1.9 dB and the global reduction was about 0.4 dB, which is significantly less than that obtained using the ideal reference source. In test 3, the reference microphone was moved more "upstream" i.e., closer to the sub-woofers. This resulted in 3.7 dB local reduction and 1.5 dB global reduction.

Tests 4–8 used two disturbance inputs, one for each sub-woofer bank, each uncorrelated. For these tests, two reference signals were used. Test 4 used the ideal reference at low disturbance levels and produced 9.3 dB local reduction and 7.7 dB global reduction. Although the complexity of the sound field increased, control was maintained and improved by using multiple references. For case 5, microphones near the sub-woofer banks were used as references. The local reduction was measured to be 4.9 dB and the global reduction was 4.7 dB. This was significantly better than for the comparable single reference case.

Tests 6–8, were conducted at higher sound pressure levels and used two ideal reference signals in each case. No tests were performed at high sound pressure levels using external microphones as reference signals. In test 6, the external load was about 117 dB, and the closed-loop reduction was measured to be 7.9 dB (local) and 7.2 (global). Although this was less than that achieved using two ideal references, the global reduction was better than that achieved using a single ideal reference (test 1). In test 7, the external load was increased to about 125 dB. The measured reduction fell to 6.6 dB (local) and 6.8 dB (global). This was the first instance in which the global reduction exceeded the local reduction. However, the difference was within the experimental uncertainty (repeatability) of the internal measurements (approximately $\pm 0.2$ dB). In the final test, the external disturbance was approximately 130 dB, the measured local reduction was 5.7 dB, and the global reduction was 6.1 dB. Again, the global reduction was greater than the local reduction and the difference was 0.4 dB ($\pm 0.2$ dB). No explanation has been determined as to why the global reduction was greater than local reduction.

As indicated in Table 2, the measured DAVA power consumption for the first five tests was less than 1 W each. The power consumption increased with increasing disturbance levels. At 130 dB, each DAVA required about 25 W. The convergence time of the controller was greater than 5 min (typically 6–7 min using zero-initialized control filters). In test 8, pre-converged control filters (from test 7) were implemented and control was achieved after a few seconds (some iteration was observed).

Figs. 21 and 22 present the closed-loop results of the spatially averaged error microphones and monitor microphones, respectively, for test 5. The results indicate that no appreciable spillover was created. Both figures show similar dynamic characteristics and are only slightly different from the SISO tests conducted earlier in the program (using different end-caps and conducted in-doors). As in the SISO tests, the controller focused on the bandwidth with the largest amplitude response, which was approximately 120–160 Hz. Little performance (local or global) was

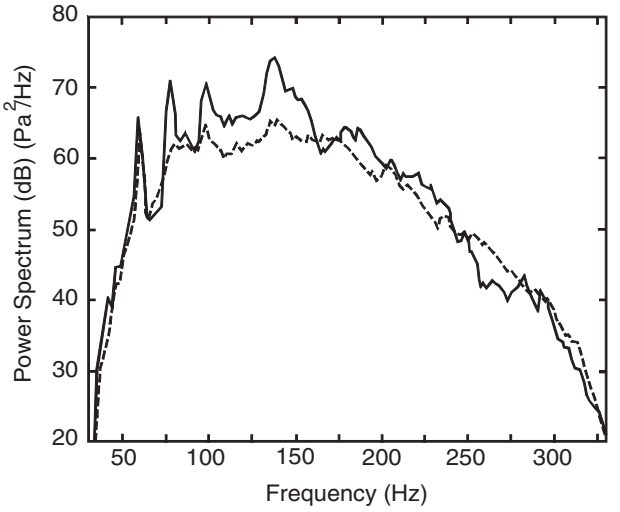


Fig. 21. Spatially averaged error microphone response for the MIMO controller: —, open-loop measurement; –– closed-loop measurement.

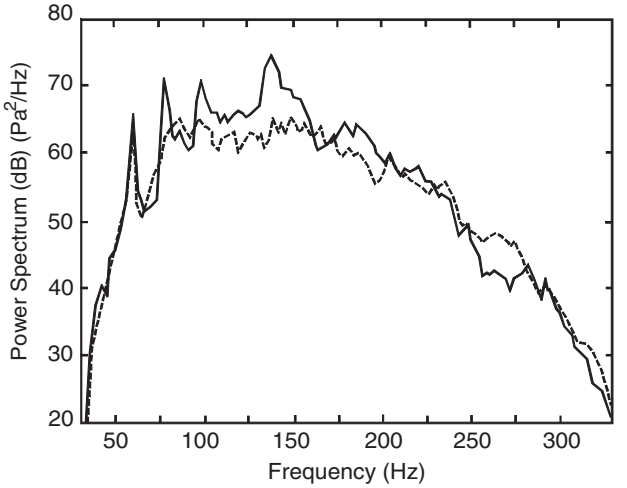


Fig. 22. Spatially averaged monitor microphone response for the MIMO controller: —, open-loop measurement; –– closed-loop measurement.

measured at the fundamental acoustic mode (~60 Hz). The noticeable roll-off resulted because of the natural roll-off of the sub-woofers and also because the tests were conducted outside in a free-field (no reverberations). Significant reduction was achieved over narrow bands around the second and third acoustic resonances. The closed-loop error response appears ''smoother'' than the closed-loop monitor response (75–150 Hz), likely because 12 error signals were averaged as opposed to 3 monitor signals. Similar trends were observed for the other test cases.

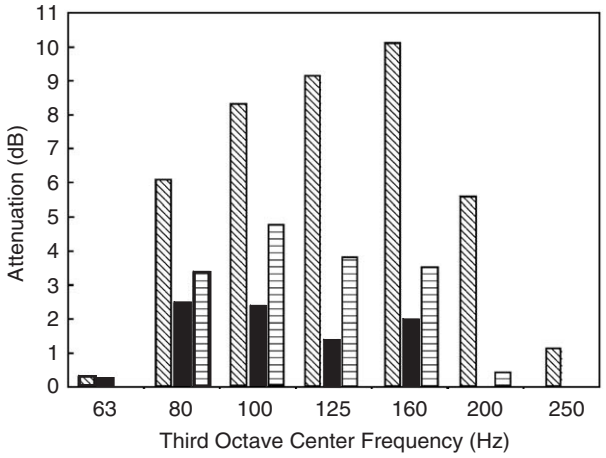


Fig. 23. Impact of reference signal on local controller performance: ▨, test #1; ■, test #2; ═, test #3.

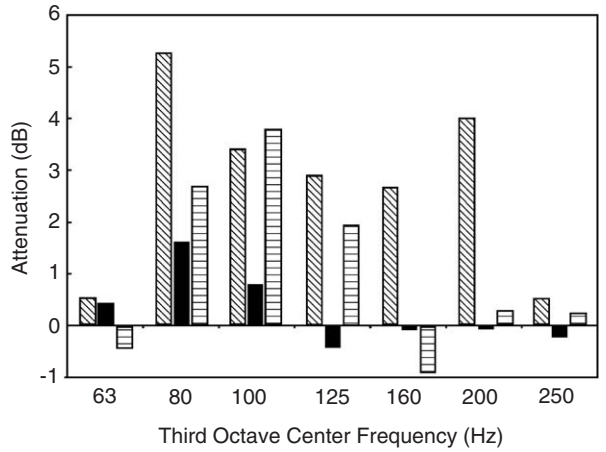


Fig. 24. Impact of reference signal on global control performance: ▨ test #1; ■, test #2; ═, test #3.

Figs. 23 and 24 present the closed-loop results for tests 1–3 (low level, single disturbance signal, single reference signal) computed over third-octave bands. These figures compare performance for the ideal reference case (test 1), a reference near the cylinder (test 2), and a reference near the disturbance source (test 3). The ideal reference provided the best local reduction in all bandwidths. For the 63 Hz bandwidth, no local reduction was measured for test 3. No local reduction was measured above the 160 Hz bandwidth for test 2. Fig. 24 shows the closed-loop performance at the monitor microphones. No spillover was measured using the ideal reference, but the other test cases show that some spillover occurred.

Figs. 25 and 26 compare the closed-loop reductions at the error and monitor microphones in third-octave bands for tests 1, 3–5. These comparisons show the effect of having an ideal reference

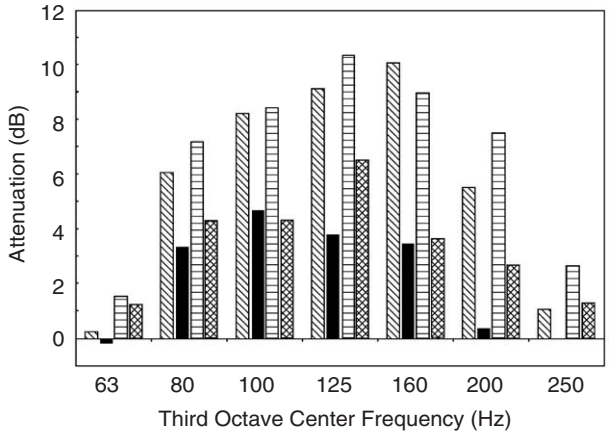


Fig. 25. Comparison of single and multiple references and disturbances on local control performance: ▨, test #1; ■, test #3; ▤, test #4; ▩, test #5.

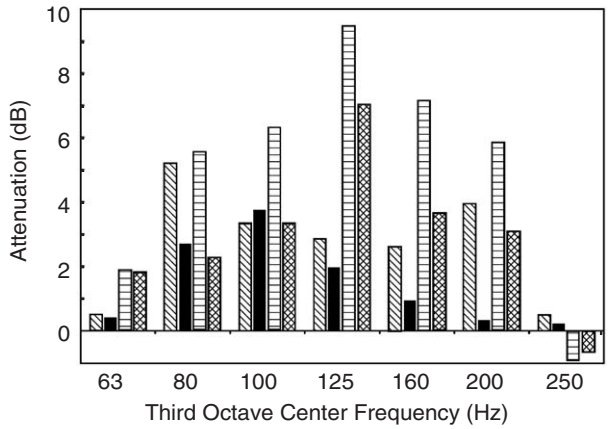


Fig. 26. Comparison of single and multiple references and disturbances on global control performance: ▨, test #1; ■, test #3; ▤, test #4; ▩, test #5.

as opposed to an upstream microphone signal, and also compare the results for a signal disturbance source to two disturbance sources. Fig. 25 shows that the error microphones measured little or no spillover. The ideal reference case provided almost twice the reduction in each bandwidth, except at 63 and 250 Hz. Reduction levels were not strongly dependent upon the number of disturbance sources and references. However, the case where two reference microphones were used did perform somewhat better than the case using only a single reference microphone. The global reductions are given in Fig. 26 and show that some spillover occurred for both microphone and ideal-tests. The best global reduction was clearly achieved using two disturbance sources with two ideal reference signals, which yielded the most reduction in all bandwidths with the exception of 250 Hz.

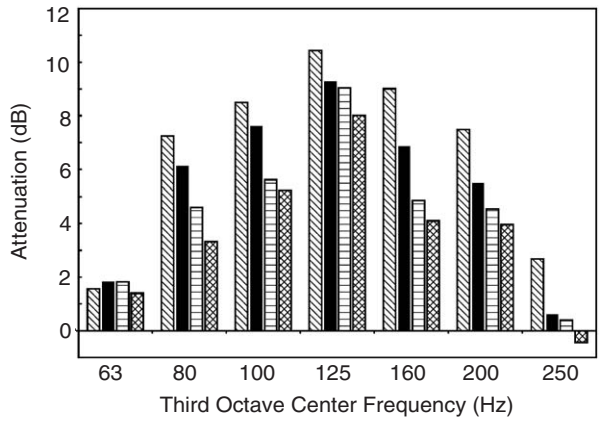


Fig. 27. Impact of disturbance level on local control performance: ▨, test #4; ■, test #6; ═, test #7; ▩, test #8.

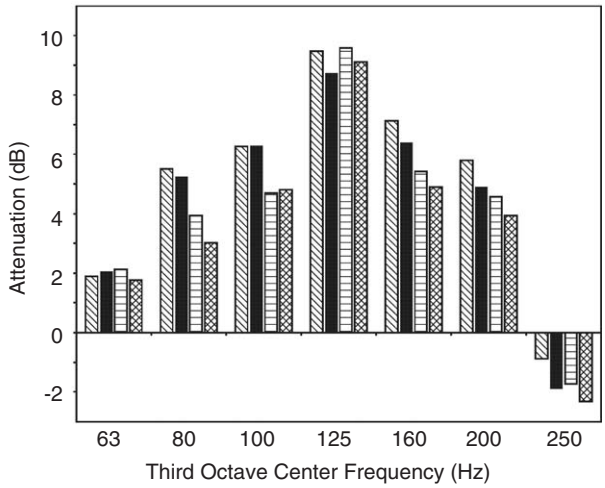


Fig. 28. Impact of disturbance level on global control performanc: ▨, test #4; ■, test #6; ═, test #7; ▩, test #8.

Figs. 27 and 28 compare the closed-loop performance in third-octaves for tests 4, 6–8, which were conducted using two disturbance signals, two ideal references, and at increasing levels. Generally, performance decreased with increasing sound pressure levels. Spillover was only measured in the 250 Hz bandwidth. Peak reductions were measured in the 125 Hz bandwidth. Since the voltage signals applied to the DAVA's were less than 25 V each (maximum operating voltage was about 30 V), the actuators were not over-driven. Rather, it is suspected that the performance rolled off due to current limits of the power amplifiers used to drive the actuators.

### 4.3. Practical implementation

The MIMO system implemented in these tests consisted of eight DAVA actuators, each having a mass of 0.22 kg. For an actual fairing application, the estimated mass for sufficient power amplifiers is estimated to be about 0.45 kg. The controller mass is estimated to be 0.9 kg, and filters/signal conditioners are estimated to be 0.15 kg. Transducers, cables, and wiring harnesses are estimated to require 0.22 kg. Necessary battery mass is estimated to be 2.0 kg. The total mass for the active control system is then at least 5.48 kg, which is approximately 12 pounds at 1-$g$ acceleration. The control system consumed about 25 W of power per DAVA at 130 dB external sound pressure level. If the disturbance load increased to 140 dB, it is estimated that the control system would still have sufficient authority, but would require about 640 W (total).

The greatest obstacle for practical implementation is the necessity of an a priori system identification of the control actuator to error transfer function paths, and a converged control filter prior to engine ignition. Typically, the distance from the engines to the fairing is much greater than the distance available in these tests, so obtaining reference signals coherent to the disturbance with sufficient phase-lead should be achievable.

## 5. Conclusions

The goal of this effort was to evaluate ASAC using DAVA actuators for noise control of composite payload fairings at realistic acoustic load levels. This work examined many important issues such as modeling, actuator performance, the importance of reference signal selection, controller convergence, local and global closed-loop performance, and implementation issues. Single-channel and multiple-channel adaptive feedforward controllers were successfully designed and implemented on a composite cylinder very similar to an actual composite fairing. Closed-loop control was demonstrated at external loads near 130 dB.

Considerable effort was expended attempting to develop an accurate coupled structural–acoustic model for the bandwidth up to 200 Hz. However, the uncertainty in structural parameters, coupling, and boundary conditions made the task of developing an accurate numerical model insurmountable. It was determined that the better choice was to rely on measured transfer functions and system identifications for understanding system dynamics and developing controllers.

The DAVA actuators developed during this program were a critical accomplishment for enabling closed-loop control at high disturbance levels. The DAVA actuators were linear to about 30 V (rms) and had an effective bandwidth of about 80–200 Hz. The DAVAs were small, lightweight, and consumed less than 24 W each at disturbance levels of 130 dB.

The controllers implemented the Filtered-X LMS algorithm, and both single- and multi-channel configurations were studied. Closed-loop performance was measured by spatially averaging error microphones for local control and monitor microphones for global control. Tests were conducted in a laboratory and outside. Dependence on reference signal selection was investigated. Tests showed that microphones placed outside of the cylinder provided a sufficiently coherent reference signal for control. The position of the reference sensor was varied and compared to an ideal reference source. The results showed that controller performance was

strongly dependent on the lead-time, or phase-lead, provided by the reference signal. Control was achieved for multiple uncorrelated disturbance sources using multiple reference signals. Greater lead-time in the reference yielded more closed-loop reduction.

Issues regarding control filter size, sample rate, and convergence speed were also investigated. The sample frequency was set between 500 and 900 Hz, which allowed for control filters and system identifications of up to 500 filter coefficients. Analysis showed that performance degraded with reduced control filter length, although no impact was observed in the SISO experiments. The multi-channel controller required several minutes to converge. However, using pre-converged control filters was demonstrated to be a viable option.

The single-channel controller produced some local closed-loop reduction, but in most test cases there was no appreciable global reduction. The multi-channel tests demonstrated both local and global control over the control bandwidth, but spillover did occur at some frequencies. In the multi-channel tests, up to 5 dB of broadband noise reduction was measured, and up to 10 dB reduction was measured in individual third-octave bands.

The most critical challenge for implementation is the necessity to compute system identification models of the many control actuator to error sensor transfer functions and obtaining a pre-converged control filter prior to launch. The weight of the control system is expected to be at least 53 N (12 lbs), much of which would be battery mass. The control system would add complexity due to the cabling for the many sensors and actuators. It is not obvious if the modest reductions observed would justify the higher cost and risk of an active control system in comparison to a purely passive foam blanket treatment.

## Acknowledgements

The authors wish to thank Haisam A. Osman of Boeing Integrated Defense Systems for collaborating on this effort and for providing the composite cylinder test structure. The authors would like to acknowledge the assistance provided by Simon Esteve, Tony Harris and Steve Booth of Virginia Tech. Finally, the authors would like to thank Steve O'Regan and Bart Burkewitz for their major contribution to the initial phase of this effort.

## References

[1] J. Higgins, E. Fosness, P. Wegner, S. Buckley, Overview of next generation composite fairing development. *ASCE SPACE 2002 Technology Conference*, March 2002.

[2] C.E. Harris, J.H. Starnes, M.J. Shuart, Design and manufacturing of aerospace composite structures state-of-the-art assessment, *Journal of Aircraft* 39 (4) (2002) 545–560.

[3] M.J. Robinson, Composite structures on the DC-XA reusable launch vehicle, *Journal of Advanced Materials* 20 (3) (1997) 9–18.

[4] A.M. Pandelli, Composite materials evolution in space launchers, Mecanique Industrielle et Materiaux 50(5) 1997.

[5] H. Osman, M. Johnson, C. Fuller, P. Marcotte, Interior noise reduction of composite cylinders using distributed vibration absorbers, Seventh *AIAA/CEAS*, Paper No. AIAA-2001-2230.

[6] S. Esteve, M. Johnson, Reduction of sound transmission into a circular cylindrical shell using distributed vibration absorbers and Helmholtz resonators, *Journal of Acoustical Society of America* 112 (6) (2002) 2840–2848.

[7] B. Gardner, M. Kidner, Enhancing low frequency transmission loss with heterogeneous acoustic blankets, *Spacecraft and Launch Vehicle Dynamic Environments Workshop*, El Segundo, CA, June 2003.
[8] N. Atalla, R. Panneton, F. Sgard, X. Olny, Acoustic absorption of macro-perforated porous materials, *Journal of Sound and Vibration* 243 (4) (2001) 659–678.
[9] S.A. Lane, J.D. Kemp, S. Griffin, R.L. Clark, Active acoustic control of a rocket fairing using spatially weighted transducer arrays, *AIAA Journal of Spacecraft and Rockets* 38 (1) (2001) 112–119.
[10] S.A. Lane, S. Griffin, D. Leo, Active structural acoustic control of a launch vehicle fairing using monolithic piezoceramic actuators, *Journal of Intelligent Material Systems and Structures* 12 (12) (2001) 795–806.
[11] S. Griffin, S.A. Lane, C. Hansen, B. Cazzolato, Active structural acoustic control of a rocket fairing using proof-mass actuators, *AIAA Journal of Spacecraft and Rockets* 38 (2) (2001) 219–225.
[12] J.D. Kemp, R.L. Clark, Noise reduction in a launch vehicle fairing using actively tuned loudspeakers, *Journal of the Acoustical Society of America* 113 (4) (2003) 1986–1994.
[13] S. Griffin, S. A. Lane, Development of a device for reduction of low frequency sound transmission reduction in small launch vehicles, *145th Meeting of the Acoustical Society of America*, Nashville, TN, April 2003.
[14] S. Griffin, A. Lazzaro, B. K. Henderson, S. A. Lane, Development of an adaptive passive vibro-acoustic device for payload fairings, *44th AIAA/ASME/ASCE/AHS Structures, Structural Dynamics, and Materials Conference*, AIAA Paper #2003-1814, April 2003.
[15] B. K. Henderson, S. A. Lane, C. Gerhart, R. Richard, Overview of the vibro-acoustic launch protection experiment at Air Force Research Laboratory, *SPIE Smart Structures and Materials Conference*, March 2003.
[16] R. Corsaro, Light weight low frequency woofer for active sound control in payload fairings, *Proceedings of the SPIE—The International Society for Optical Engineering* 4332 (2001) 254–258.
[17] R. Glaese, E. Anderson, Active structural–acoustic control for composite payload fairing, *Proceedings of the SPIE—The International Society for Optical Engineering* 3668 (1–2) (1999) 450–461.
[18] C. Niezrecki, H. Cudney, Feasibility to control launch vehicle internal acoustics using piezoelectric actuators, *Journal of Intelligent Material Systems and Structures*, Vol. 12(9) September 2001, pp. 647–660.
[19] C. Guigou, C. Fuller, Control of aircraft interior broadband noise with foam-PVDF smart skin, *Journal of Sound and Vibration* 220 (3) (1999) 541–557.
[20] J. Griffin, M. Johnson, C. Fuller, Active control of transmission of turbulent boundary layer noise using smart foam elements, Journal of the Acoustical Society of America 104(3) (Part 2) (1998) 1851.
[21] C. Fuller, C. Rogers, C. Liang, Active foam for noise and vibration control, U.S. Patent No. 5,719,945, 1998.
[22] P. Gardonio, N. Ferguson, F. Fahy, Modal expansion analysis of noise transmission through circular cylindrical shell structure with blocking masses, *Journal of Sound and Vibration* (2001).
[23] Matlab Software, Rel. 12, The Mathworks Inc, Natick, MA, 2004.
[24] F. Fahy, *Sound and Structural Vibration*, Academic Press, London UK, 1985, pp. 249-245.
[25] D. Morgan, C. Sanford, A control theory approach to the stability and transient analysis of the filtered-x LMS adaptive notch filter, *IEEE Transactions on Signal Processing* 40 (9) (1992) 2341–2346.
[26] S. Snyder, C. Hansen, The effect of transfer function estimation errors on the filtered-x LMS algorithm, *IEEE Transactions on Signal Processing* 42 (4) (1994) 950–953.
[27] R. L. Clark, W. R. Saunders, G. P. Gibbs, *Adaptive Structures, Dynamics and Control*, Wiley, New York, 1998, pp. 330–337.
[28] J.N. Juang, *Applied System Identification*, Prentice-Hall, Englewood Cliffs, NJ, 1994.
[29] S. Haykin, *Adaptive Filter Theory*, Prentice-Hall, Englewood Cliffs, NJ, 1986.
[30] PCB Model 130C10, sensitivity = 21.6 mV/Pa, dynamic range = 20 to 7000 Hz $\pm 1$ dB, linearity $<3\%$ $>128$ dB SPL.
[31] Radian Audio Engineering woofer model 2218, 46-cm diameter, 600 W RMS, sensitivity = 96 dB at 1 W at 1 m, frequency range = 45 Hz to 3.5 kHz, closed cabinet, volume $\sim 0.5$ m$^3$.
[32] B. Widrow, S. Stearns, *Adaptive Signal Processing*, Prentice-Hall, Englewood Cliffs, NJ, 1985.